

Nucleon to  $\Delta$  axial and pseudoscalar transition form factorsChen Chen<sup>ID, 1,2</sup> Christian S. Fischer<sup>ID, 3,4</sup> and Craig D. Roberts<sup>ID, 5,6</sup><sup>1</sup>Interdisciplinary Center for Theoretical Study, University of Science and Technology of China, Hefei, Anhui 230026, China<sup>2</sup>Peng Huanwu Center for Fundamental Theory, Hefei, Anhui 230026, China<sup>3</sup>Institut für Theoretische Physik, Justus-Liebig-Universität Gießen, D-35392 Gießen, Germany<sup>4</sup>Helmholtz Forschungsakademie Hessen für FAIR (HFHF),

GSI Helmholtzzentrum für Schwerionenforschung, Campus Gießen, 35392 Gießen, Germany

<sup>5</sup>School of Physics, Nanjing University, Nanjing, Jiangsu 210093, China<sup>6</sup>Institute for Nonperturbative Physics, Nanjing University, Nanjing, Jiangsu 210093, China

Email: chenchen1031@ustc.edu.cn (CC); christian.fischer@theo.physik.uni-giessen.de (CSF); cdroberts@nju.edu.cn (CDR)

(Dated: 2023 December 21)

A symmetry-preserving continuum approach to the calculation of baryon properties in relativistic quantum field theory is used to predict all form factors associated with nucleon-to- $\Delta$  axial and pseudoscalar transition currents, thereby unifying them with many additional properties of these and other baryons. The new parameter-free predictions can serve as credible benchmarks for use in analysing existing and anticipated data from worldwide efforts focused on elucidation of  $\nu$  properties.

*1. Introduction* — With the discovery of neutrino ( $\nu$ ) masses twenty-five years ago [1–3], science acquired tangible evidence of phenomena that lie beyond the Standard Model of particle physics (SM). With such motivation, precision measurements of  $\nu$ ,  $\bar{\nu}$  (antineutrino) properties are today amongst the top priorities in fundamental physics [4–11].

Known neutrinos are very weakly interacting; so, their detection requires excellent understanding of detector responses to  $\nu$  passage. The array of interactions that can occur depends strongly on  $\nu$  energy. At low energies, elastic scattering on entire nuclei dominates; whereas at high energies, individual neutrons and protons (nucleons) are resolved and deep inelastic  $\nu$ -parton scatterings take place. (Partons are the degrees-of-freedom used to define quantum chromodynamics – QCD, *i.e.*, the SM theory of strong interactions.) Yet another class of reactions is important in few-GeV reactor-based  $\nu$  experiments, *viz.* inelastic processes on single or small clusters of nucleons, which produce a range of excited-nucleon final states.

To some extent, the required cross-sections can be determined in dedicated  $\nu$  scattering experiments. However, reliable strong interaction theory predictions are equally important. In this context, results for nucleon ( $N$ ) electroweak elastic and transition form factors become critical to interpreting modern  $\nu$  oscillation experiments [12–15]. Recognising this, the past five years have seen a focus on calculating the form factors associated with elastic  $\nu N$  scattering using both continuum and lattice Schwinger function methods [16–20].

However, as noted above, inelastic processes are also crucial to understanding existing and anticipated experiments. The most significant of these are excitations of the  $\Delta$ -resonance via, *e.g.*,  $\nu_\ell N \rightarrow \ell \Delta$  and  $\nu_\ell N \rightarrow \ell(\pi N \rightarrow \Delta)$ , where  $\ell$  is a light lepton and the second process involves the  $\pi$ -meson [21, 22]. Only one set of related calculations exists [23, 24]. They were obtained using lattice-QCD (lQCD) with quark current masses that produce a pion mass-squared  $m_\pi^2 \gtrsim 5(m_\pi^{\text{empirical}})^2$ ,

$m_\pi^{\text{empirical}} = 0.135 \text{ GeV}$ . Lacking further studies, challenges remain, like extending computations to  $m_\pi^{\text{empirical}}$  and significantly reducing all uncertainties.

Hitherto, there have been no more recent predictions. We address that lack herein, employing a continuum approach to the baryon bound-state problem that has widely been used with success [25–28]. Of particular relevance are its unifying predictions for  $N$  and  $\Delta$ -baryon elastic weak-interaction form factors [16, 17, 29]. Where comparisons with experiment and results obtained using other robust tools are available, there is agreement.

*2. Axial and pseudoscalar currents* — Weak  $N \rightarrow \Delta$  transitions are described by the matrix element

$$\mathcal{J}_{5\mu}^j(K, Q) := \langle \Delta(P_f; s_f) | \mathcal{A}_{5\mu}^j(0) | N(P_i; s_i) \rangle \quad (1a)$$

$$= \bar{u}_\alpha(P_f; s_f) \Gamma_{5\mu, \alpha}^j(K, Q) u(P_i; s_i), \quad (1b)$$

where  $P_{i,j}(s_{i,j})$  are the momenta (spins) of the incoming nucleon and outgoing  $\Delta$ , respectively, which are on-shell:  $P_{i,f}^2 = -m_{N,\Delta}^2$ ; and  $K = (P_f + P_i)/2$ ,  $Q = P_f - P_i$ . Isospin symmetry is assumed throughout [30]; and the on-shell baryons are described by Dirac and Rarita-Schwinger spinors, respectively – see Ref. [31, Appendix B] for details. Introducing the column vector  $\psi = \text{column}[u, d]$ , with  $u, d$  being the two light-flavour quark fields, then the axial current operator may be written  $\mathcal{A}_{5\mu}^j(x) = \bar{\psi}(x) \frac{\tau^j}{2} \gamma_5 \gamma_\mu \psi(x)$ , in which the isospin structure is expressed via the Pauli matrices  $\{\tau^j | j = 1, 2, 3\}$ .

Owing to the assumed isospin symmetry, a complete characterisation of  $N \rightarrow \Delta$  weak transitions can be achieved by focusing solely on the neutral current ( $j = 3$ )  $p \rightarrow \Delta^+$  transition, in which case the vertex is typically written in the following form [32, 33]:

$$\Gamma_{5\mu, \alpha}^3(K, Q) = \sqrt{\frac{2}{3}} \left[ i(\gamma_\mu Q_\alpha - \delta_{\mu\alpha} Q) C_3^A(Q^2)/m_N - (\delta_{\mu\alpha}(P_f \cdot Q) - P_{f\mu} Q_\alpha) C_4^A(Q^2)/m_N^2 + \delta_{\mu\alpha} C_5^A(Q^2) - Q_\mu Q_\alpha C_6^A(Q^2)/m_N^2 \right], \quad (2)$$

where  $C_{3,4,5,6}^A$  are the four Poincaré-invariant transition form factors and  $\sqrt{2/3}$  is the isospin coefficient.

The related pseudoscalar transition matrix element is

$$\mathcal{J}_5^j(K, Q) = \langle \Delta(P_f; s_f) | \mathcal{P}_5^j(0) | N(P_i; s_i) \rangle \quad (3a)$$

$$= \bar{u}_\alpha(P_f; s_f) \Gamma_{5,\alpha}^j(Q) u(P_i; s_i), \quad (3b)$$

where  $\mathcal{P}_5^j(x) = \bar{\psi}(x) \frac{\tau^j}{2} \gamma_5 \psi(x)$ . For the neutral current:

$$\Gamma_{5,\alpha}^3(Q) = \sqrt{\frac{2}{3}} i \frac{Q_\alpha}{4m_N} \frac{m_\pi^2}{Q^2 + m_\pi^2} \frac{f_\pi}{m_q} G_{\pi N \Delta}(Q^2). \quad (4)$$

Here,  $G_{\pi N \Delta}$  is the pseudoscalar transition form factor,  $m_q$  is the light-quark current-mass, and  $f_\pi = 0.092 \text{ GeV}$  is the pion leptonic decay constant [34].

Using the PCAC (partially conserved axial current) identity [30]:  $\partial_\mu \mathcal{A}_{5\mu}^j(x) + 2m_q \mathcal{P}_5^j(x) = 0$ , one obtains the following ‘‘off-diagonal’’ PCAC relation:

$$C_5^A(Q^2) - \frac{Q^2}{m_N^2} C_6^A(Q^2) = \frac{f_\pi m_\pi^2 / [2m_N]}{Q^2 + m_\pi^2} G_{\pi N \Delta}(Q^2). \quad (5)$$

Drawing a parallel with the nucleon [16],  $C_5^A$  is kindred to the nucleon’s axial form factor,  $G_A$ , and  $C_6^A$  to its induced-pseudoscalar form factor,  $G_P$ . Since  $Q^2 C_6^A(Q^2)|_{Q^2=0} = 0$ , one immediately obtains the off-diagonal Goldberger-Treiman (GT) relation

$$2m_N C_5^A(0) = f_\pi G_{\pi N \Delta}(0). \quad (6)$$

As consequences of chiral symmetry and its breaking pattern, only frameworks preserving Eqs. (5), (6) are viable.

*3. Baryon structure* — The structure of any given baryon can be described by a Faddeev amplitude, obtained from a Poincaré-covariant Faddeev equation that sums all possible exchanges and interactions which can occur between the three dressed-quarks that characterise its valence content. Studies of the associated scattering problem reveal that there is no interaction contribution from the diagram in which each leg of the three-gluon vertex ( $3gV$ ) is attached to a separate quark [26, Eq.(2.2.10)]. Thus, whilst the  $3gV$  is a primary factor in generating the process-independent QCD effective charge [35, 36], its role within baryons is largely to produce tight quark + quark (diquark) correlations. Consequently, the baryon bound-state problem may reliably be transformed [37–39] into solving the homogeneous matrix equation in Fig. 1.

Each line and vertex in Fig. 1 is specified in Ref. [16], which delivers parameter-free predictions for the nucleon  $G_{A,P}$  form factors and unifies them with the pion-nucleon form factor,  $G_{\pi NN}$ . A key to the success of that study is a sound expression of emergent hadron mass and its corollaries [27, 40–45], such as a running light-quark mass whose value at infrared momenta,  $M_D \approx 0.4 \text{ GeV}$ , defines the natural magnitude for mass-dimensioned quantities in the light-quark sector of the Standard Model. Associated mass-scales for the isoscalar-scalar and isovector-axialvector diquarks are [in GeV]:

$$m_{\{ud\}} = 0.80, \quad m_{\{uu\}} = m_{\{ud\}} = m_{\{dd\}} = 0.89. \quad (7)$$

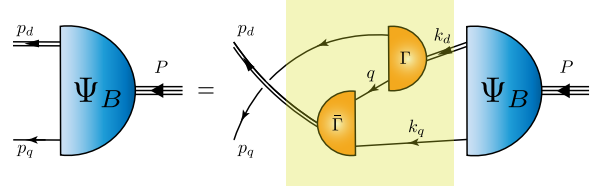


FIG. 1. Faddeev integral equation, whose solution is the Poincaré-covariant matrix-valued function  $\Psi_B$ , the Faddeev amplitude for a baryon  $B$  with total momentum  $P = p_q + p_d$ . Legend. *Shaded box* – Faddeev kernel; *single line* – dressed-quark propagator;  $\Gamma$  – diquark correlation amplitude; and *double line* – diquark propagator. Only isoscalar-scalar diquarks,  $\{ud\}$ , and isovector-axialvector diquarks,  $\{uu\}$ ,  $\{dd\}$  play a material role in nucleons and  $\Delta$ -baryons [26].

In computing all transition form factors, we follow Refs. [16, 17, 29]: they are obtained from the nucleon elastic weak form factor expressions by replacing all inputs connected with the final state by those for the  $\Delta$ -baryon. The normalisations of the  $N$  and  $\Delta$  Faddeev amplitudes are available from Refs. [16, 29]. (The interaction current is included with the supplemental material.)

*4. Dominant  $N \rightarrow \Delta$  transition axial form factors* —  $C_{5,6}^A$  in Eq. (2) are dominant in the axial transition current. Our prediction for  $C_5^A(x = Q^2/\bar{m}^2)$ ,  $\bar{m} = [m_N + m_\Delta]/2$ , is drawn in Fig. 2A. On the domain depicted,  $C_5^A(x)$  can fairly be interpolated using a dipole characterised by the  $x = 0$  value and axial mass listed in the first row of Table I. The  $x = 0$  value is 0.94(5)-times the prediction for  $g_A$ , the nucleon axial coupling, as calculated using the same framework; and the axial mass is 0.95(3)-times the analogous scale in a dipole representation of  $G_A(x)$ , the nucleon axial form factor, *viz.* the axial transition form factor is softer, something also found in a coupled channels analysis of axial  $N \rightarrow \Delta$  transitions [21].

The reported uncertainty in our predictions expresses the impact of  $\pm 5\%$  variations of the diquark masses in Eq. (7). The results obtained from independent variations are combined with weight fixed by the relative strength of scalar ( $0^+$ ) and axialvector ( $1^+$ ) diquark contributions to  $C_5^A(0)$ , *i.e.*, approximately 4:1. Like the nucleon case [16, 17], the  $0^+$  and  $1^+$  mass variations interfere destructively, *e.g.*, reducing  $m_{\{ud\}}$  increases  $C_5^A(0)$ , whereas  $C_5^A(0)$  decreases with the same change in  $m_{1^+}$ .

In phenomenology, following Ref. [47], it has been common to represent  $C_5^A$  as follows [46]:

$$C_5^A(Q^2) = C_5^A(0) \frac{[1 + a_5 Q^2 / (b_5 + Q^2)]}{(1 + Q^2 / \bar{m}_A^2)^2}, \quad (8)$$

where  $C_5^A(0) = 1.2$ ,  $a_5 = -1.21$ ,  $b_5 = 2 \text{ GeV}^2$  are parameters discussed in Ref. [47]. The value of  $C_5^A(0)$  is an estimate based on the off-diagonal GT relation – Eq. (6). Using Eq. (8) and the same functional form for  $C_{3,4,6}^A$ , then a fit to  $\nu d \rightarrow \mu^- \Delta^{++n}$  bubble chamber data yielded the value of  $\bar{m}_A$  in Table I.

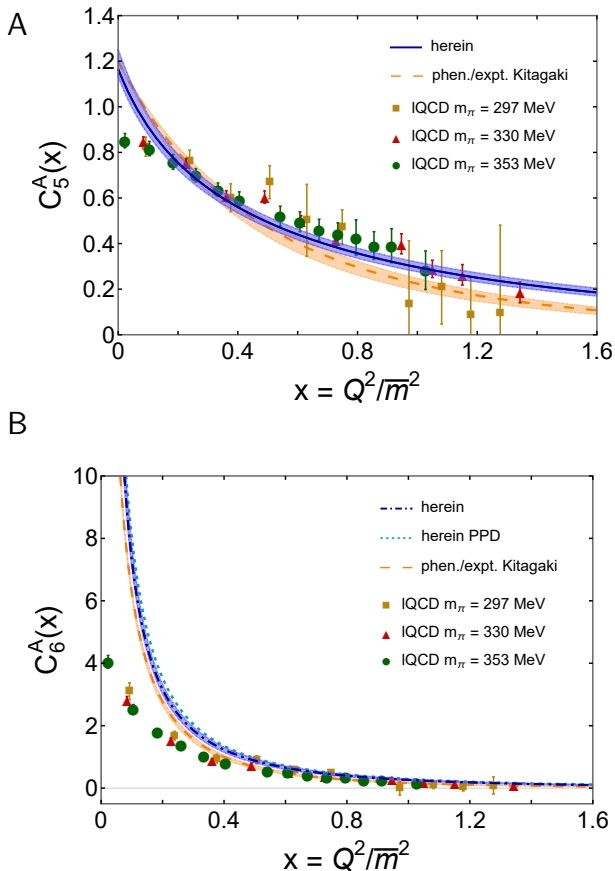


FIG. 2. Panel A.  $C_5^A$  calculated herein – blue curve within lighter blue uncertainty band; and empirical result [46, Kitagaki] – dashed orange curve within uncertainty band. Panel B.  $C_6^A$  calculated herein – dot-dashed blue curve within uncertainty band; dotted cyan curve – PPD approximation, Eq. (9), using our prediction for  $C_5^A(x)$ ; and dashed orange curve within uncertainty band – PPD approximation obtained with empirical result [46] for  $C_5^A(x)$ . Both panels: IQCD [23, 24] – hybrid (HYB) [green circles –  $m_\pi = 353$  MeV] and domain wall fermions (DWF) [gold squares –  $m_\pi = 297$  MeV, red triangles –  $m_\pi = 330$  MeV]. (Parametrisations of our form factor predictions are provided in the supplemental material.)

Taken at face value, this result is 1.34(17)-times that which some phenomenological estimates now associate with the nucleon axial form factor [48]. However, as noted above, such estimates are based on dipole parametrisations. If one recasts Eq. (8) as a dipole, then the empirical fit corresponds to  $\tilde{m}_A = 1.01(5)m_N = 0.878(41)\bar{m}$  – we have listed this value in Row 3 of Table I. Using an  $\mathcal{L}_1$  measure, then, on the phenomenological fitting domain  $Q^2 \in [0, 3]$  GeV<sup>2</sup>, the curves thus obtained agree with the original parametrisations to within 7.6(1.1)%. This dipole mass scale is 0.70(3)-times that associated with the nucleon  $G_A$ .

Our prediction for  $C_5^A$  in Fig. 2A is contrasted therein with a phenomenological/empirical result [46] and IQCD computations [23, 24]. Allowing for the constraint im-

TABLE I. Selected characteristics of  $C_5^A$  compared with combined phenomenology and experiment [46] and other available calculations [23, 24]. ( $2\tilde{m} = m_N + m_\Delta$ .)

	$C_5^A(0)$	$\tilde{m}_A/\bar{m}$
Herein	$1.16_{-0.03}^{+0.09}$	1.01(2)
Phenomenology/Empirical [46]	1.2	1.18(8)
Phenomenology/Empirical (dipole)	1.2	0.88(4)
IQCD [23] $m_\pi = 353$ MeV	0.90(1)	1.32(3)
IQCD [24] $m_\pi = 297$ MeV	0.94(6)	1.32(13)
IQCD [24] $m_\pi = 330$ MeV	0.97(3)	1.23(5)

posed on data analysis by working with Eq. (8), the existing phenomenological extraction agrees well with our prediction. Regarding the IQCD results, however, there are significant differences. Compared to our prediction and phenomenology, the IQCD results lie lower on  $x \simeq 0$  and are harder – these differences are quantified in Table I. It seems fair to judge that these discrepancies owe primarily to the larger than physical pion masses which characterise the lattice configurations.

We draw our prediction for  $C_6^A(x)$  in Fig. 2B, wherein it is compared with available IQCD computations. In this case, too, the IQCD results lie low on  $x \lesssim 0.4$  and are harder than our prediction.

Since  $C_6^A$  is kindred to the nucleon induced pseudoscalar form factor,  $G_P$ , it is natural to expect that a pion pole dominance (PPD) approximation is also valid for the  $N$ - $\Delta$  axial transition. Referring to Eq. (5), this off-diagonal PPD approximation is ( $\mu_N \equiv m_N^2/\bar{m}^2$ ,  $\mu_\pi \equiv m_\pi^2/\bar{m}^2$ )

$$C_6^A(x) \approx C_5^A(x)\mu_N/[x + \mu_\pi]. \quad (9)$$

Figure 2B reveals it to be a quantitatively reliable association, just as its analogues are for the nucleon and  $\Delta$ -baryon weak elastic form factors [16, 29]. (Additional information is provided in the supplemental material.)

*5. Subdominant  $N \rightarrow \Delta$  transition form factors* — Our predictions for  $C_{3,4}^A$  are drawn in Fig. 3A and compared with the phenomenological extractions [46]: the models used therein assume  $C_3^A \equiv 0$  and  $C_4^A = -C_5^A/4$ . Our predictions disagree markedly with those assumptions.

$C_3^A$  is the weak  $N \rightarrow \Delta$  analogue of the electric quadrupole ( $E2$ ) form factor in  $\gamma N \rightarrow \Delta$  transitions [49, 50]. Like the vector  $E2$  transition strength, if the nucleon and  $\Delta$ -baryon are described by SU(6) symmetric (spherical) wave functions, then  $C_3^A \equiv 0$ . Evidently, in our Poincaré covariant treatment,  $C_3^A \neq 0$ . Indeed, no Poincaré-covariant  $N$  or  $\Delta$ -baryon wave function is simply S-wave in character – see, *e.g.*, the wave functions in Ref. [51]. We find  $C_3^A(x)$  decreases monotonically with increasing  $x$  from a maximum value  $C_3^A(0) = 0.26_{-0.04}^{+0.17}$ .

Considering Fig. 3A, our prediction for  $C_4^A$  exhibits qualitatively similar behaviour to the phenomenological parametrisation. Quantitatively, however, it is uniformly

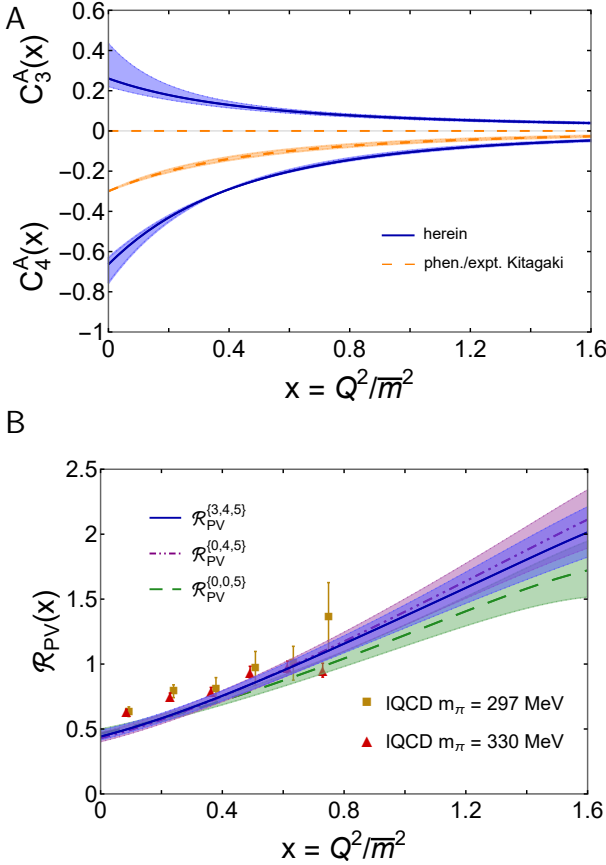


FIG. 3. Panel A. Predictions for subdominant transition form factors – blue curves within bracketing uncertainty band:  $C_4^A(x)$ , negative curves; and  $C_3^A(x)$ , non-negative curves. Both cases: empirical extraction [46, Kitagaki] – dashed orange curve and bracketing band. Panel B. PV ratio, Eq. (10): legend superscript indicates transition form factors retained in the calculation. For comparison, IQCD results [24]: gold squares –  $m_\pi = 297$  MeV, red triangles –  $m_\pi = 330$  MeV.

larger in magnitude: we predict  $C_4^A(0) = -0.66_{-0.10}^{+0.03}$ , versus  $C_4^A(0) = -0.3$  in the parametrisation.

**6. Parity violation asymmetry** — With the construction and use of high-luminosity facilities, spin observables can today be used to probe hadron structure and search for beyond-SM physics – see, *e.g.*, Refs. [52–54]. One such quantity is the parity-violating asymmetry in electroweak excitation of the  $\Delta$ -baryon [55]:

$$\mathcal{R}_{PV}^{\{3,4,5\}}(Q^2) := \frac{C_5^A}{C_3^A} \left[ 1 + \frac{m_\Delta^2 - Q^2 - m_N^2}{2m_N^2} \frac{C_4^A}{C_5^A} - \frac{m_N^2 + Q^2 + 2m_N m_\Delta - 3m_\Delta^2}{4m_N m_\Delta} \frac{C_3^A}{C_5^A} \right]. \quad (10)$$

Having calculated the weak  $N \rightarrow \Delta$  transition form factors, in Fig. 3B we deliver a prediction for this as yet unmeasured ratio. Since  $\pi N$  final-state interactions play a material role in understanding the low- $x$  behaviour of  $\gamma N \rightarrow \Delta$  transition form factors [56] and such effects are

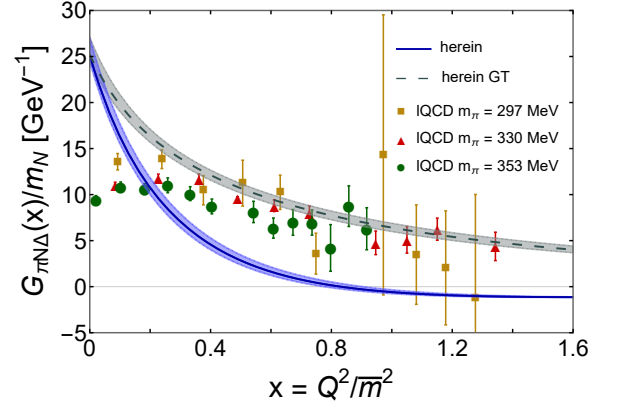


FIG. 4.  $G_{\pi N \Delta}(x)/m_N$  calculated herein – blue curve within uncertainty band;  $G'_{\pi N \Delta}(x)/m_N$  – dashed grey curve and band, where our result for  $C_5^A(x)$  is used on the right in Eq. (12). Comparison: IQCD [23, 24] – hybrid [green circles –  $m_\pi = 353$  MeV] and domain wall fermions [gold squares –  $m_\pi = 297$  MeV, red triangles –  $m_\pi = 330$  MeV]. Our prediction for  $G_{\pi N \Delta}(-m_\pi^2)/m_N = 27.43_{-0.68}^{+2.02}$  is consistent with that obtained using chiral perturbation theory [58].

difficult to represent reliably – see, *e.g.*, Ref. [31, Sec. 6], we use our predictions for  $C_{3,4,5}^A$  but construct  $C_3^V$  from the parametrisations presented in Ref. [57, MAID].

Two principal conclusions may be drawn from Fig. 3B: (i)  $\mathcal{R}_{PV}(0) = 0.45(4) > 0$ , which may be compared with a value of  $\approx 0.6$  if one uses the empirical parametrisations from Ref. [46]; and (ii)  $C_5^A$  is dominant on  $x \lesssim 0.5$ , but  $C_{3,4}^A$  become increasingly important as  $x$  grows.

**7. Pseudoscalar transition form factor** — Our prediction for  $G_{\pi N \Delta}$  is drawn in Fig. 4. Defined as usual, the  $G_{\pi N \Delta}$  radius is  $r_{\pi N \Delta} = 1.4(1) r_{\pi N N}$ , where  $r_{\pi N N}$  is the  $G_{\pi N N}$  analogue [16]. Our prediction is softer than available IQCD results. Notably, owing to a persistent negative contribution from probe seagull couplings to the diquark-quark vertices, we find a zero in  $G_{\pi N \Delta}$  at  $x = 0.84(6)$ . (See Fig. 5 and Table II in the supplemental material.) Given the large pion masses and poor precision, extant IQCD results cannot test this prediction.

It is clear from Fig. 4 that the GT relation, Eq. (6), is satisfied: specifically [in 1/GeV],

$$\frac{G_{\pi N \Delta}(0)}{m_N} = 25.2_{-0.7}^{+1.9} \text{ cf. } \frac{2C_5^A(0)}{f_\pi} = 25.1_{-0.6}^{+1.9}. \quad (11)$$

As with nucleon and  $\Delta$  elastic weak form factors, the GT relation is only valid on  $x \simeq 0$ . Symmetry guarantees nothing more. We highlight this in Fig. 4 by also plotting

$$G'_{\pi N \Delta}(x)/m_N := (2/f_\pi) C_5^A(x). \quad (12)$$

Plainly,  $G'_{\pi N \Delta}(x) \approx G_{\pi N \Delta}(x)$  only on  $x \lesssim 0.1$ . (Additional remarks on PCAC are contained in the supplemental material.)

**8. Summary** — Using a Poincaré-covariant, symmetry-preserving treatment of the continuum baryon bound-

state problem, in which all elements possess an unambiguous link with analogous quantities in QCD, we delivered parameter-free predictions for every form factor associated with  $N \rightarrow \Delta$  transitions driven by axial or pseudoscalar probes. In doing so, we completed a unified description of, *inter alia*, all  $N$  and/or  $\Delta$ -baryon axial-vector and pseudoscalar currents. Where comparisons with data are available, our predictions are confirmed. Hence, the results herein can serve as a reliable resource for use in analysing existing and anticipated data relevant to worldwide efforts focused on elucidation of  $\nu$ ,  $\bar{\nu}$  prop-

erties. No material improvement upon our results may be envisaged before the same array of observables can be calculated using either the explicit three-body Poincaré-covariant Faddeev equation approach to  $N$ ,  $\Delta$  elastic and transition form factors or numerical simulations of lQCD.

*Acknowledgments*—We are grateful for constructive communications with K. Graczyk, T.-S.H. Lee, A. Lovato and T. Sato. Work supported by: National Natural Science Foundation of China (grant nos. 12135007, 12247103); and Deutsche Forschungsgemeinschaft (grant no. FI 970/11-1).

- 
- [1] Y. Fukuda, et al., Evidence for oscillation of atmospheric neutrinos, *Phys. Rev. Lett.* 81 (1998) 1562–1567.
- [2] T. Kajita, Nobel Lecture: Discovery of atmospheric neutrino oscillations, *Rev. Mod. Phys.* 88 (2016) 030501.
- [3] A. B. McDonald, Nobel Lecture: The Sudbury Neutrino Observatory: Observation of flavor change for solar neutrinos, *Rev. Mod. Phys.* 88 (2016) 030502.
- [4] L. Alvarez-Ruso, et al., NuSTEC White Paper: Status and challenges of neutrino–nucleus scattering, *Prog. Part. Nucl. Phys.* 100 (2018) 1–68.
- [5] C. A. Argüelles, et al., New opportunities at the next-generation neutrino experiments I: BSM neutrino physics and dark matter, *Rept. Prog. Phys.* 83 (12) (2020) 124201.
- [6] B. Abi, et al., Long-baseline neutrino oscillation physics potential of the DUNE experiment, *Eur. Phys. J. C* 80 (10) (2020) 978.
- [7] J. A. Formaggio, A. L. C. de Gouvêa, R. G. H. Robertson, Direct Measurements of Neutrino Mass, *Phys. Rept.* 914 (2021) 1–54.
- [8] A. Abusleme, et al., JUNO physics and detector, *Prog. Part. Nucl. Phys.* 123 (2022) 103927.
- [9] A. Lokhov, S. Mertens, D. S. Parno, M. Schlösser, K. Valerius, Probing the Neutrino-Mass Scale with the KATRIN Experiment, *Ann. Rev. Nucl. Part. Sci.* 72 (2022) 259–282.
- [10] L. A. Ruso, et al., Theoretical tools for neutrino scattering: interplay between lattice QCD, EFTs, nuclear physics, phenomenology, and neutrino event generators – arXiv:2203.09030 [hep-ph] .
- [11] M. Sajjad Athar, A. Fatima, S. K. Singh, Neutrinos and their interactions with matter, *Prog. Part. Nucl. Phys.* 129 (2023) 104019.
- [12] U. Mosel, Neutrino Interactions with Nucleons and Nuclei: Importance for Long-Baseline Experiments, *Ann. Rev. Nucl. Part. Sci.* 66 (2016) 171–195.
- [13] R. J. Hill, P. Kammel, W. J. Marciano, A. Sirlin, Nucleon Axial Radius and Muonic Hydrogen — A New Analysis and Review, *Rept. Prog. Phys.* 81 (2018) 096301.
- [14] P. Gysbers, et al., Discrepancy between experimental and theoretical  $\beta$ -decay rates resolved from first principles, *Nature Phys.* 15 (5) (2019) 428–431.
- [15] A. Lovato, J. Carlson, S. Gandolfi, N. Rocco, R. Schiavilla, Ab initio study of  $(\nu_\ell, \ell^-)$  and  $(\bar{\nu}_\ell, \ell^+)$  inclusive scattering in  $^{12}\text{C}$ : confronting the MiniBooNE and T2K CCQE data, *Phys. Rev. X* 10 (2020) 031068.
- [16] C. Chen, C. S. Fischer, C. D. Roberts, J. Segovia, Nucleon axial-vector and pseudoscalar form factors and PCAC relations, *Phys. Rev. D* 105 (9) (2022) 094022.
- [17] C. Chen, C. D. Roberts, Nucleon axial form factor at large momentum transfers, *Eur. Phys. J. A* 58 (2022) 206.
- [18] C. Alexandrou, M. Constantinou, K. Hadjiyiannakou, K. Jansen, C. Kallidonis, G. Koutsou, A. Vaquero Aviles-Casco, Nucleon axial form factors using  $N_f = 2$  twisted mass fermions with a physical value of the pion mass, *Phys. Rev. D* 96 (2017) 054507.
- [19] Y.-C. Jang, R. Gupta, B. Yoon, T. Bhattacharya, Axial Vector Form Factors from Lattice QCD that Satisfy the PCAC Relation, *Phys. Rev. Lett.* 124 (2020) 072002.
- [20] G. S. Bali, L. Barca, S. Collins, M. Gruber, M. Löffler, A. Schäfer, W. Söldner, P. Wein, S. Weishäupl, T. Wurm, Nucleon axial structure from lattice QCD, *JHEP* 05 (2020) 126 (2020).
- [21] T. Sato, D. Uno, T. S. H. Lee, Dynamical model of weak pion production reactions, *Phys. Rev. C* 67 (2003) 065201.
- [22] D. Simons, N. Steinberg, A. Lovato, Y. Meurice, N. Rocco, M. Wagman, Form factor and model dependence in neutrino-nucleus cross section predictions – arXiv:2210.02455 [hep-ph] .
- [23] C. Alexandrou, G. Koutsou, T. Leontiou, J. W. Negele, A. Tsapalis, Axial Nucleon and Nucleon to Delta form factors and the Goldberger-Treiman Relations from Lattice QCD, *Phys. Rev. D* 76 (2007) 094511, [Erratum: *Phys. Rev. D* 80, 099901 (2009)].
- [24] C. Alexandrou, G. Koutsou, J. W. Negele, Y. Proestos, A. Tsapalis, Nucleon to Delta transition form factors with  $N_F = 2 + 1$  domain wall fermions, *Phys. Rev. D* 83 (2011) 014501.
- [25] G. Eichmann, H. Sanchis-Alepuz, R. Williams, R. Alkofer, C. S. Fischer, Baryons as relativistic three-quark bound states, *Prog. Part. Nucl. Phys.* 91 (2016) 1–100.
- [26] M. Y. Barabanov, et al., Diquark Correlations in Hadron Physics: Origin, Impact and Evidence, *Prog. Part. Nucl. Phys.* 116 (2021) 103835.
- [27] M. Ding, C. D. Roberts, S. M. Schmidt, Emergence of Hadron Mass and Structure, *Particles* 6 (1) (2023) 57–120.
- [28] D. S. Carman, R. W. Gothe, V. I. Mokeev, C. D. Roberts, Nucleon Resonance Electroexcitation Amplitudes and Emergent Hadron Mass, *Particles* 6 (1) (2023) 416–439.

- [29] P.-L. Yin, C. Chen, C. S. Fischer, C. D. Roberts,  $\Delta$ -Baryon axialvector and pseudoscalar form factors, and associated PCAC relations, *Eur. Phys. J. A* 59 (7) (2023) 163.
- [30] C. Itzykson, J.-B. Zuber, *Quantum Field Theory*, McGraw-Hill Inc., New York, 1980.
- [31] J. Segovia, I. C. Cloet, C. D. Roberts, S. M. Schmidt, Nucleon and  $\Delta$  elastic and transition form factors, *Few Body Syst.* 55 (2014) 1185–1222.
- [32] S. L. Adler, Photoproduction, electroproduction and weak single pion production in the (3,3) resonance region, *Annals Phys.* 50 (1968) 189–311.
- [33] C. H. Llewellyn Smith, Neutrino Reactions at Accelerator Energies, *Phys. Rept.* 3 (1972) 261–379.
- [34] R. L. Workman, et al., Review of Particle Physics, *PTEP* 2022 (2022) 083C01.
- [35] Z.-F. Cui, J.-L. Zhang, D. Binosi, F. de Soto, C. Mezrag, J. Papavassiliou, C. D. Roberts, J. Rodríguez-Quintero, J. Segovia, S. Zafeiropoulos, Effective charge from lattice QCD, *Chin. Phys. C* 44 (2020) 083102.
- [36] A. Deur, S. J. Brodsky, C. D. Roberts, QCD Running Couplings and Effective Charges, *Prog. Part. Nucl. Phys.* 134 (2024) 104081.
- [37] R. T. Cahill, C. D. Roberts, J. Praschifka, Baryon structure and QCD, *Austral. J. Phys.* 42 (1989) 129–145.
- [38] H. Reinhardt, Hadronization of Quark Flavor Dynamics, *Phys. Lett. B* 244 (1990) 316–326.
- [39] G. V. Efimov, M. A. Ivanov, V. E. Lyubovitskij, Quark - diquark approximation of the three quark structure of baryons in the quark confinement model, *Z. Phys. C* 47 (1990) 583–594.
- [40] C. D. Roberts, D. G. Richards, T. Horn, L. Chang, Insights into the emergence of mass from studies of pion and kaon structure, *Prog. Part. Nucl. Phys.* 120 (2021) 103883.
- [41] D. Binosi, Emergent Hadron Mass in Strong Dynamics, *Few Body Syst.* 63 (2) (2022) 42.
- [42] G. Salmè, Explaining mass and spin in the visible matter: the next challenge, *J. Phys. Conf. Ser.* 2340 (1) (2022) 012011.
- [43] G. F. de Teramond, Emergent phenomena in QCD: The holographic perspective – arXiv:2212.14028 [hep-ph], in: 25th Workshop on What Comes Beyond the Standard Models?, 2022.
- [44] M. N. Ferreira, J. Papavassiliou, Gauge Sector Dynamics in QCD, *Particles* 6 (1) (2023) 312–363.
- [45] G. Krein, Femtoscopy of the Matter Distribution in the Proton, *Few Body Syst.* 64 (3) (2023) 42.
- [46] T. Kitagaki, et al., Study of  $\nu d \rightarrow \mu^- pp_s$  and  $\nu d \rightarrow \mu^- \Delta^{++} n_s$  using the BNL 7-foot deuterium filled bubble chamber, *Phys. Rev. D* 42 (1990) 1331–1338.
- [47] P. A. Schreiner, F. Von Hippel, Neutrino production of the Delta (1236), *Nucl. Phys. B* 58 (1973) 333–362.
- [48] A. S. Meyer, M. Betancourt, R. Gran, R. J. Hill, Deuterium target data for precision neutrino-nucleus cross sections, *Phys. Rev. D* 93 (2016) 113015.
- [49] J. Liu, N. C. Mukhopadhyay, L.-s. Zhang, Nucleon to delta weak excitation amplitudes in the nonrelativistic quark model, *Phys. Rev. C* 52 (1995) 1630–1647.
- [50] D. Barquilla-Cano, A. J. Buchmann, E. Hernandez, Axial  $N \rightarrow \Delta(1232)$  and  $N \rightarrow N^*(1440)$  transition form factors, *Phys. Rev. C* 75 (2007) 065203, [Erratum: *Phys.Rev.C* 77, 019903 (2008)].
- [51] L. Liu, C. Chen, Y. Lu, C. D. Roberts, J. Segovia, Com-  
position of low-lying  $J = \frac{3}{2}^\pm$   $\Delta$ -baryons, *Phys. Rev. D* 105 (11) (2022) 114047.
- [52] D. Androic, et al., The G0 Experiment: Apparatus for Parity-Violating Electron Scattering Measurements at Forward and Backward Angles, *Nucl. Instrum. Meth. A* 646 (2011) 59–86.
- [53] D. Becker, et al., The P2 experiment, *Eur. Phys. J. A* 54 (11) (2018) 208.
- [54] J. Arrington, et al., The solenoidal large intensity device (SoLID) for JLab 12 GeV, *J. Phys. G* 50 (11) (2023) 110501.
- [55] N. C. Mukhopadhyay, M. J. Ramsey-Musolf, S. J. Pollock, J. Liu, H. W. Hammer, Parity violating excitation of the Delta (1232): Hadron structure and new physics, *Nucl. Phys. A* 633 (1998) 481–518.
- [56] B. Julia-Diaz, T. S. H. Lee, T. Sato, L. C. Smith, Extraction and Interpretation of  $\gamma N \rightarrow \Delta$  Form Factors within a Dynamical Model, *Phys. Rev. C* 75 (2007) 015205.
- [57] D. Drechsel, S. S. Kamalov, L. Tiator, Unitary Isobar Model - MAID2007, *Eur. Phys. J. A* 34 (2007) 69–97.
- [58] Y. Ünal, A. Küçükarslan, S. Scherer, Axial-vector nucleon-to-delta transition form factors using the complex-mass renormalization scheme, *Phys. Rev. D* 104 (9) (2021) 094014.

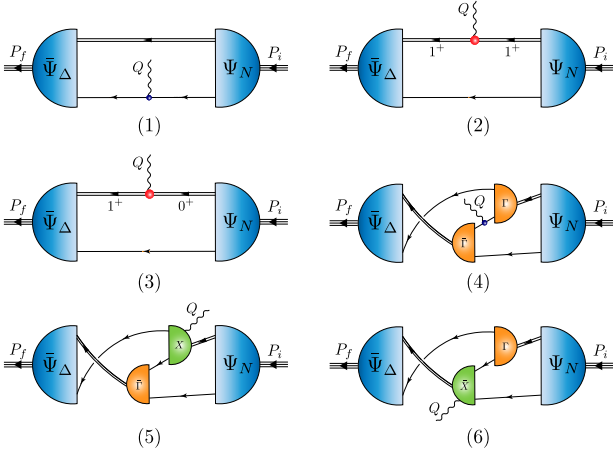


FIG. 5. Symmetry-preserving axial/pseudoscalar current for on-shell baryons ( $B = N, \Delta$ ) that are described by the Faddeev amplitudes  $\Psi_B$  obtained by solving the equation depicted in Fig. 1. *Single line* – dressed-quark propagator; *undulating line* – axial/pseudoscalar current;  $\Gamma$  – diquark correlation amplitude; *double line* – diquark propagator; and  $\chi$  – seagull terms.

..... *Supplemental Material* .....

This material is included with a view to illustrating/exemplifying remarks in the main text, including, in some cases, numerical confirmation of observations inferred from figures, and supplying practicable representations of the form factor predictions.

Within the quark + diquark picture of baryons, the axial and pseudoscalar currents, Eqs. (1b) and (4), can both be decomposed into a sum of six terms, depicted in Fig. 5. Evidently, the probe interacts with the dressed-quarks and -diquarks in various ways, each of which is detailed in Ref. [16, Sec. IIIC]. Referring to Fig. 5, in Table II we list the relative strength of each diagram’s contribution to  $C_{3,4,5,6}^A(0)$  and  $G_{\pi N\Delta}(0)$ .

In order to assist others in employing our predictions for the form factors associated with nucleon-to- $\Delta$  axial and pseudoscalar transition currents, here we present practicable parametrisations, valid as interpolations and useful for extrapolation. We considered a range of options, achieving good results with the following functional forms:

$$\mathcal{F}(x) = \frac{n_{\mathcal{F}}^0 + n_{\mathcal{F}}^1 x / (n_{\mathcal{F}}^2 + x)^2}{(1 + d_{\mathcal{F}}^1 x)^2}, \quad (13)$$

for  $\mathcal{F} = C_{i=3,4,5}^A$ ;

$$C_6^A(x) = \frac{n_{C_6^A}^0 + n_{C_6^A}^1 x / (n_{C_6^A}^2 + x)^2}{(1 + d_{C_6^A}^1 x)^2} \frac{\mu_N}{x + \mu_\pi}, \quad (14)$$

reflecting PPD, Eq. (9); and

$$G_{\pi N\Delta}/m_N = \frac{n_G^0 + n_G^1 x}{1 + d_G^1 x + d_G^2 x^2 + d_G^3 x^3}. \quad (15)$$

TABLE II. Referring to Fig. 5, separation of the axial-vector form factors  $C_i^A(0)$  ( $i = 3, 4, 5, 6$ ), and the  $\pi N\Delta$  form factor  $G_{\pi N\Delta}(0)$  into contributions from various diagrams, listed as a fraction of the total  $Q^2 = 0$  value. Diagram (1):  $\langle J \rangle_q^A$  – weak- or pseudoscalar-probe strikes dressed-quark with axialvector diquark spectator. Diagram (2):  $\langle J \rangle_{qq}^{AA}$  – probe strikes axialvector diquark with dressed-quark spectator. Diagram (3):  $\langle J \rangle_{qq}^{AS}$  – probe mediates scalar to axialvector diquark transition, with dressed-quark spectator. Diagram (4):  $\langle J \rangle_{ex}$  – probe strikes dressed-quark “in-flight” between one diquark correlation and another. Diagrams (5) and (6):  $\langle J \rangle_{sg}$  – probe couples inside the diquark correlation amplitude. The listed uncertainties reflect the impact of  $\pm 5\%$  variations in the diquark masses in Eq. (7), *e.g.*,  $-0.116_{\mp} \Rightarrow -0.11 \mp 0.06$ .

	$\langle J \rangle_q^A$	$\langle J \rangle_{qq}^{AA}$	$\langle J \rangle_{qq}^{AS}$	$\langle J \rangle_{ex}$	$\langle J \rangle_{sg}$
$C_5^A(0)$	$0.489_{\pm}$	$0.0175_{\pm}$	$0.211_{\pm}$	$0.2910_{\mp}$	0
$C_6^A(0)$	$0.509_{\pm}$	$0.0165_{\pm}$	$0.211_{\pm}$	$0.528_{\mp}$	$-0.252_{\mp}$
$C_3^A(0)$	$-0.115_{\pm}$	$0.1412_{\pm}$	$0.3710_{\pm}$	$0.6027_{\mp}$	0
$C_4^A(0)$	$0.448_{\pm}$	$0.05237_{\pm}$	$0.232_{\pm}$	$0.2810_{\mp}$	0
$G_{\pi N\Delta}(0)$	$0.5311_{\pm}$	$0.0204_{\pm}$	$0.172_{\pm}$	$0.5710_{\mp}$	$-0.293_{\mp}$

TABLE III. Interpolation parameters for the  $N \rightarrow \Delta$  axial and pseudoscalar transition form factors, for use in Eqs. (15), (14). All dimensionless, except  $n_G^{0,1}$ , the numerator coefficients for  $G_{\pi N\Delta}/m_N$  in Eq. (15), which are listed in  $\text{GeV}^{-1}$ .

	$C_5^A$	$C_6^A$	$C_3^A$	$C_4^A$	$G_{\pi N\Delta}/m_N$
$n^0$	$1.16^{+0.09}_{-0.03}$	$1.43^{+0.17}_{-0.10}$	$0.26^{+0.17}_{-0.04}$	$-0.66^{+0.03}_{-0.10}$	$25.15^{+1.90}_{-0.67}$
$n^1$	$-0.27^{+0.19}_{-0.07}$	$-0.22^{+0.13}_{-0.03}$	$-0.87^{+0.34}_{-0.35}$	$7.85^{+1.22}_{-0.84}$	$-30.29^{+0.34}_{-1.27}$
$n^2$	$0.46^{+0.05}_{-0.07}$	$0.17^{+0.02}_{-0.03}$	$2.02^{+1.25}_{-0.68}$	$3.67^{+0.35}_{-0.46}$	
$d^1$	$0.87^{+0.06}_{-0.06}$	$1.06^{+0.01}_{-0.01}$	$0.62^{+0.33}_{-0.17}$	$0.70^{+0.12}_{-0.24}$	$3.31^{+0.01}_{-0.15}$
$d^2$					$2.53^{+0.22}_{-0.15}$
$d^3$					$1.88^{+0.58}_{-0.36}$

All interpolation coefficients are listed in Table III.

The off-diagonal PPD approximation is written in Eq. (9). Here we choose to supplement Fig. 2 with additional quantitative information. Consider, therefore, the following ratio

$$R_{PPD} := \frac{\mu_N C_5^A}{(x + \mu_\pi) C_6^A}. \quad (16)$$

The calculated result is depicted in Fig. 6. The  $x$ -dependence of  $R_{PPD}$  is very much like the analogous curves obtained for the nucleon [16, Fig. 8] and the  $\Delta(1232)$ -baryon [29, Fig. 8]: it lies  $< 2.5\%$  below unity on  $x \simeq 0$  and grows toward unity as  $x$  increases. The explanation for the accuracy and behaviour of this approximating formula can be found, *e.g.*, in Ref. [29, Sec. 4.3].

Some corollaries of PCAC were discussed in connection with Eqs. (11), (12). As done separately for the nucleon and  $\Delta$ -baryon weak elastic form factors [16, 29], they may be extended. Indeed, following Ref. [29, Sec. 4.3], one can

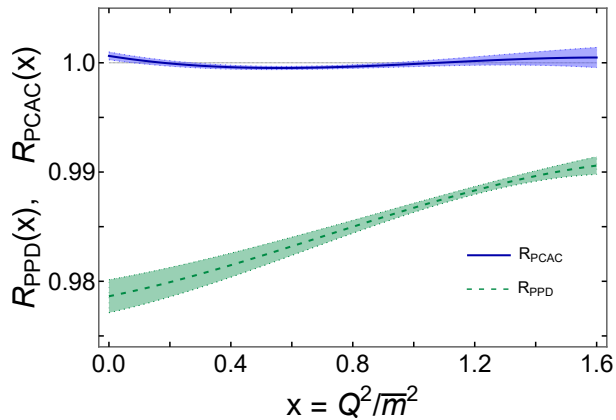


FIG. 6. Quantitative verification of the accuracy of the PPD approximation – Eq. (16): dashed green curve within lighter band; and numerical verification of the PCAC relation – Eq. (17): solid blue curve within lighter band.

prove algebraically that  $C_5^A$ ,  $C_6^A$ , and  $G_{\pi N \Delta}$  satisfy the off-diagonal PCAC relation, Eq. (5), as they must in any symmetry preserving treatment of  $N \rightarrow \Delta$  weak transitions. Thus, the PCAC ratio

$$R_{PCAC} := \frac{2m_N \mu_N C_5^A}{2m_N x C_6^A + \mu_N \mu_\pi f_\pi G_{\pi N \Delta} / (x + \mu_\pi)}, \quad (17)$$

should be unity. We draw the numerical result for this ratio in Fig. 6: evidently, allowing for numerical accuracy, the curve is indistinguishable from unity. The uncertainty band highlights that the result is parameter-independent.